Received: 7 December 2018 | Revised: 20 March 2019 | Accepted: 15 April 2019

DOI: 10.1002/mrm.27803

FULL PAPER

Magnetic Resonance in Medicine

Nonuniform Fourier-decomposition MRI for ventilation- and perfusion-weighted imaging of the lung

David Bondesson[1,2] | Moritz J. Schneider[1,2] | Thomas Gaass[3] | Bernd Kühn[4] | Grzegorz Bauman[5,6] | Olaf Dietrich[1] | Julien Dinkel[1,2]

[1]Department of Radiology, University Hospital, LMU Munich, Munich, Germany

[2]Comprehensive Pneumology Center (CPC-M), German Center for Lung Research (DZL), Munich, Germany

[3]Siemens Healthcare Pty Ltd, Bowen Hills, Australia

[4]Siemens Healthcare GmbH, Erlangen, Germany

[5]Division of Radiological Physics, Department of Radiology, University of Basel Hospital, Basel, Switzerland

[6]Department of Biomedical Engineering, University of Basel, Basel, Switzerland

Correspondence
David Bondesson, Marchioninistr. 15, Munich, Bavaria, Germany 81377.
Email: david.bondesson@med.uni-muenchen.de

Funding information
The authors acknowledge partial funding by the German Center for Lung Research (DZL), but received no specific grant for this research from any funding agency in the public, commercial or not-for-profit sector.

Purpose: To improve the robustness of pulmonary ventilation- and perfusion-weighted imaging with Fourier decomposition (FD) MRI in the presence of respiratory and cardiac frequency variations by replacing the standard fast Fourier transform with the more general nonuniform Fourier transform.

Theory and Methods: Dynamic coronal single-slice MRI of the thorax was performed in 11 patients and 5 healthy volunteers on a 1.5T whole-body scanner using a 2D ultra-fast balanced steady-state free-precession sequence with temporal resolutions of 4-9 images/s. For the proposed nonuniform Fourier-decomposition (NUFD) approach, the original signal with variable physiological frequencies that was acquired with constant sampling rate was retrospectively transformed into a signal with (ventilation or perfusion) frequency-adapted sampling rate. For that purpose, frequency tracking was performed with the synchro-squeezed wavelet transform. Ventilation- and perfusion-weighted NUFD amplitude and signal delay maps were generated and quantitatively compared with regularly sampled FD maps based on their signal-to-noise ratio (SNR).

Results: Volunteers and patients showed statistically significant increases of SNR in frequency-adapted NUFD results compared to regularly sampled FD results. For ventilation data, the mean SNR increased by 43.4% ± 25.3% and 24.4% ± 31.9% in volunteers and patients, respectively; for perfusion data, SNR increased by 93.0% ± 36.1% and 75.6% ± 62.8%. Two patients showed perfusion signal in pulmonary areas with NUFD that could not be imaged with FD.

Olaf Dietrich and Julien Dinkel contributed equally to this work.

Conclusion: This study demonstrates that using nonuniform Fourier transform in combination with frequency tracking can significantly increase SNR and reduce frequency overlaps by collecting the signal intensity onto single frequency bins.

KEYWORDS
Fourier decomposition, lung, nonuniform Fourier transform, pulmonary MRI

1 | INTRODUCTION

Pulmonary Fourier-decomposition (FD) MRI is a noninvasive free-breathing imaging method for extracting functional information about ventilation and perfusion in the lung.[1] FD MRI works on a registered series of dynamically acquired MR images of the lung, in which periodic signal changes associated with perfusion and ventilation can be spectrally separated and subsequently analyzed. Both signal variations are correlated with proton density variations, which are caused by changes in capillary blood filling (together with intravoxel dephasing effects) or changes in alveoli density, respectively.[2-4]

Several studies have shown the FD method to be a viable tool for spotting local pulmonary pathologies[5,6] without requirement of contrast-agent administration (neither intravenous agents for perfusion nor gaseous agents for ventilation assessment) or the health risks of radiation-based methods (as, e.g., CT or single photon emission CT). Inaddition to mapping the spectral amplitude, it has also been suggested that the phase information obtained by FD MRI could potentially be used for estimating the signal arrival time. The phase difference (between 2 voxels) of a single spectral frequency component is proportional to the temporal shift of the signals. Consequently, the signal arrival time (i.e., the "signal delay") can be mapped by evaluating the phase difference compared to a starting point. Thus, localized delays of spatial signal propagation caused by pathologies such as cystic fibrosis, chronic obstructive pulmonary disease, chronic thromboembolic pulmonary hypertension (CTEPH), asthma, or idiopathic pulmonary fibrosis[7,8] could be displayed.

However, inevitable random variations of respiratory or cardiac frequencies during free-breathing pulmonary measurements can be reason for artificial signal loss when using the established FD MRI approach. Related methods that have been proposed to overcome this problem require complex multiple-step post-processing including peak finding, exact phase estimation and data resorting of k-space[9] or image-space data[10] to use all of the measured signal variations as well as recalibrate the signal contribution to a single frequency.

The purpose of this study was to return to the conceptual simplicity of the initially proposed FD method and to improve its robustness (quantified in terms of signal-to-noise ratio [SNR] maps) in the presence of frequency variations by replacing the well-known fast Fourier transform with the more general nonuniform fast Fourier transform (NUFFT). This nonuniform Fourier-decomposition (NUFD) approach requires transforming the original, evenly sampled signal with variablefrequency into a signal with constant frequency that is sampled at varying rate.

2 | THEORY

In almost all real-time ventilation and perfusion measurements, signal frequencies vary nonlinearly over time. When calculating the Fourier transform, this will not only spread the resulting intensity over multiple frequency bins, but also cause phase errors if spectral content overlaps. In the following sections, an approach is described to correct for such frequency variations.

2.1 | Signal sampling

In the following, we consider an oscillating signal $S(t)$ with varying frequency $f(t)$ and assume that $S(t)$ is sampled at equidistant sampling times $t_n = n\Delta t$ with the constant sampling interval Δt. If the signal frequency $f(t)$ is varying, then the numbers of sample points t_n per signal cycle will change correspondingly (cf. Figure 1A). However, by transforming the original sampling times t_n (together with the sampled signal intensities) to "virtual," nonequidistant sampling times $\tilde{t}_n$, the same sampled intensities appear as the time course of a virtual single-frequency signal $\tilde{S}(\tilde{t})$ (cf. Figure 1B). Thus, a uniformly sampled signal with variable frequency can be transformed into a nonuniformly sampled signal with constant frequency.

The calculation of the appropriate virtual, nonequidistant sampling times $\tilde{t}_n$ can be based on the instantaneous frequency $f(t)$ of the signal, which can be determined byappropriate frequency-tracking techniques as described below. To obtain identical virtual cycle durations of $\tilde{S}(\tilde{t})$, the n-th sampling intervals $\Delta\tilde{t}_n$ must be modified proportional to the tracked frequency

$$\Delta\tilde{t}_n = \Delta t \frac{f\left(t_n\right)}{f_{\text{mean}}} \tag{1}$$

resulting in the new sampling times

$$\tilde{t}_n = \sum_{k=1}^{n} \Delta\tilde{t}_k = \frac{\Delta t}{f_{\text{mean}}} \sum_{k=1}^{n} f\left(t_k\right) \tag{2}$$

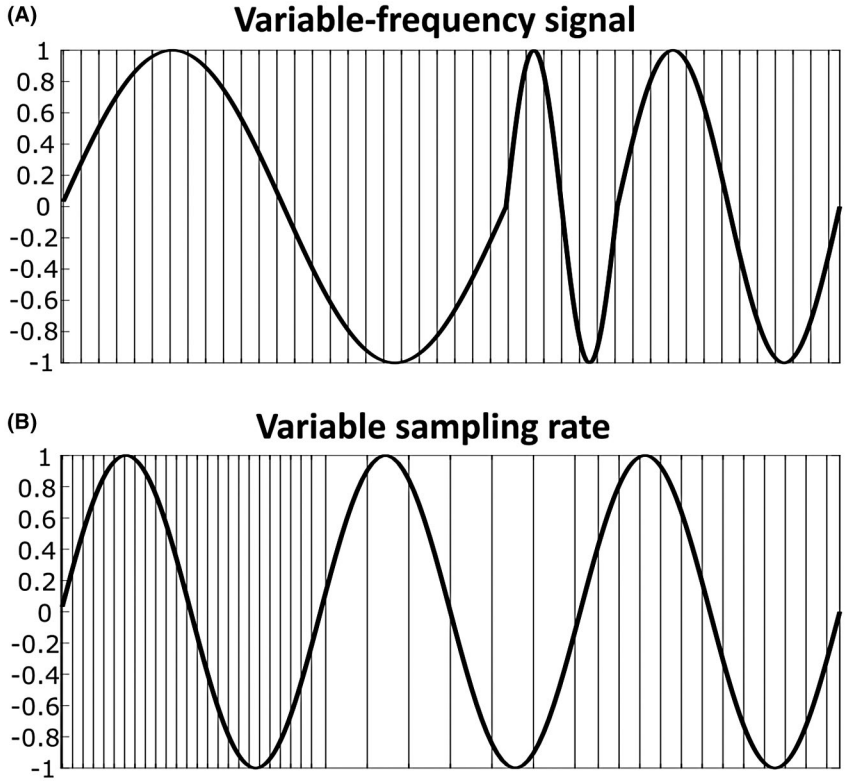

FIGURE 1 Constant and frequency-adapted sampling rate. A, Variable-frequency signal with constant sampling rate; the frequency varies every signal cycle. B, Constant-frequency signal with variable sampling rates; the same signal as above has been transformed into a constant-frequency signal by appropriately modifying the sampling rates

The scaling factor f_{mean} is to be chosen such that the total sampling duration remains the same, i.e. $\tilde{t}_N - \tilde{t}_1 = t_N - t_1$. Assuming $\tilde{t}_1 = t_1 = 0$, this is achieved by setting f_{mean} to the mean value of the tracked frequency:

$$f_{\text{mean}} = \frac{1}{N}\sum_{k=1}^{N} f\left(t_k\right). \tag{3}$$

2.2 | NUFFT

Based on the new (virtual) sampling times $\tilde{t}_n$, the selected frequency component F_k (containing, e.g., the ventilation or the perfusion component of a pulmonary measurement) of the signal $\tilde{S}(\tilde{t})$ can be quantified by Fourier analysis. However, because the sampling times $\tilde{t}_n$ are not equidistant, this cannot be done using standard FFT algorithms; instead, a type-1 NUFFT is required to calculate the (equidistant) frequency spectrum of a signal defined at nonequidistant time points.[a] The type-1 discrete nonuniform Fourier transform is defined as

$$F_k = \text{NUFFT}\left(\tilde{S}\left(\tilde{t}_n\right)\right) = \sum_{n=1}^{N} \tilde{S}\left(\tilde{t}_n\right) \exp\left(-2\pi i k \tilde{t}_n / \left(\tilde{t}_N - \tilde{t}_1\right)\right) \tag{4}$$

This looks similar to a regular discrete Fourier transform with the modification that the sampling times $\tilde{t}_n$ are not evenly spaced.

3 | METHODS

3.1 | Image acquisition

Five healthy volunteers (24-28 years old; 2 female and 3 male) and 11 patients (5 with suspicion of CTEPH, 4 with suspicion of idiopathic pulmonary arterial hypertension (PAH) and 2 with suspicion of idiopathic pulmonary fibrosis, 31-84 years old; 5 female and 6 male) underwent non–contrast-enhanced MRI under free-breathing conditions. None of the healthy volunteers were smokers. Participants were measured as preparation and part of a study (registration number NCT02791282) and written informed consent was obtained from all subjects. Patients with pulmonary hypertension were referred to the study by means of the pneumology department with no other exclusion criteria than being able to undergo 25 min of measurement; thus, only the most severe cases were excluded. MRI was performed on a 1.5T whole-body scanner (Siemens Magnetom Aera, Siemens Healthineers, Erlangen, Germany) with an 18-channel body array coil and 16 elements of a spine array coil. Functional MRI data were acquired in supine position (head first) for a single coronal mid-lung slice per subject. Dynamic single-slice imaging was performed with a 2D ultra-fast balanced steady-state free-precession (uf-bSSFP) sequence,[11] optimized to distinguish signal variations in the lung parenchyma. The main pulse sequence parameters were as follows: field of view = 450 × 450 mm^2, matrix = 96 × 96 voxels, slice thickness = 15 mm, repetition time = 1.03 ms, echo time = 0.36 ms,

flip angle: 24.5° for volunteers and 24.5-80° for patients. For volunteers, the temporal resolution was 115 ms/image, the series consisted of 1024 images, resulting in total measurement times of 117s. For the patients, the temporal resolution varied between 115 and 216 ms/image, the series consisted of 200 to 1024 images, resulting in total measurement times between 40 and 117 s.

One of the 5 healthy test subject measurements was repeated 6 times with changing amounts of frequency variability between them to investigate the stability of the compensation. The frequency variability was simply yielded by asking the test subject to change their ventilation rate more or less within each measurement. Due to respiratory sinus arrhythmia[12] increased necessity for frequency tracking in both perfusion and ventilation signal components was expected.

3.2 | Image processing workflow

A prototype software, fMRLung 4.5 (Siemens Digital Services, Princeton, NJ) was used to apply a nonrigid registration algorithm[13,14] to the measured image series. The reference image was chosen manually based on the mean value of the diaphragm signal in the apical–basal direction to yield mid-ventilation position.

All further image processing was performed with Matlab (The MathWorks, Natick, MA). The first 20 images were discarded due to transient signal behavior of the uf-bSSFP sequence. In every voxel, the DC signal was subtracted from the time signal to focus purely on the variations. A region of interest (ROI) was manually segmented (with function 'roipoly, Matlab version 2018a) along the pleural lines covering both pulmonary veins as well as parenchyma collecting both average perfusion and ventilation signal variations. Subject-specific bandpass filtering was applied to separate ventilation and perfusion components similar to the standard FD method. Additional high pass filtering was applied on the ventilation-weighted signal to remove frequencies below 0.07 Hz (corresponding to signal periods longer than 14 s), which were considered baseline drift being substantially slower than realistic breathing (Figure 2A).

Frequency tracking of the resulting signal-time course was performed with the synchro-squeezed wavelet transform (SWT) method (function "wsst", Matlab version 2018a),[15]

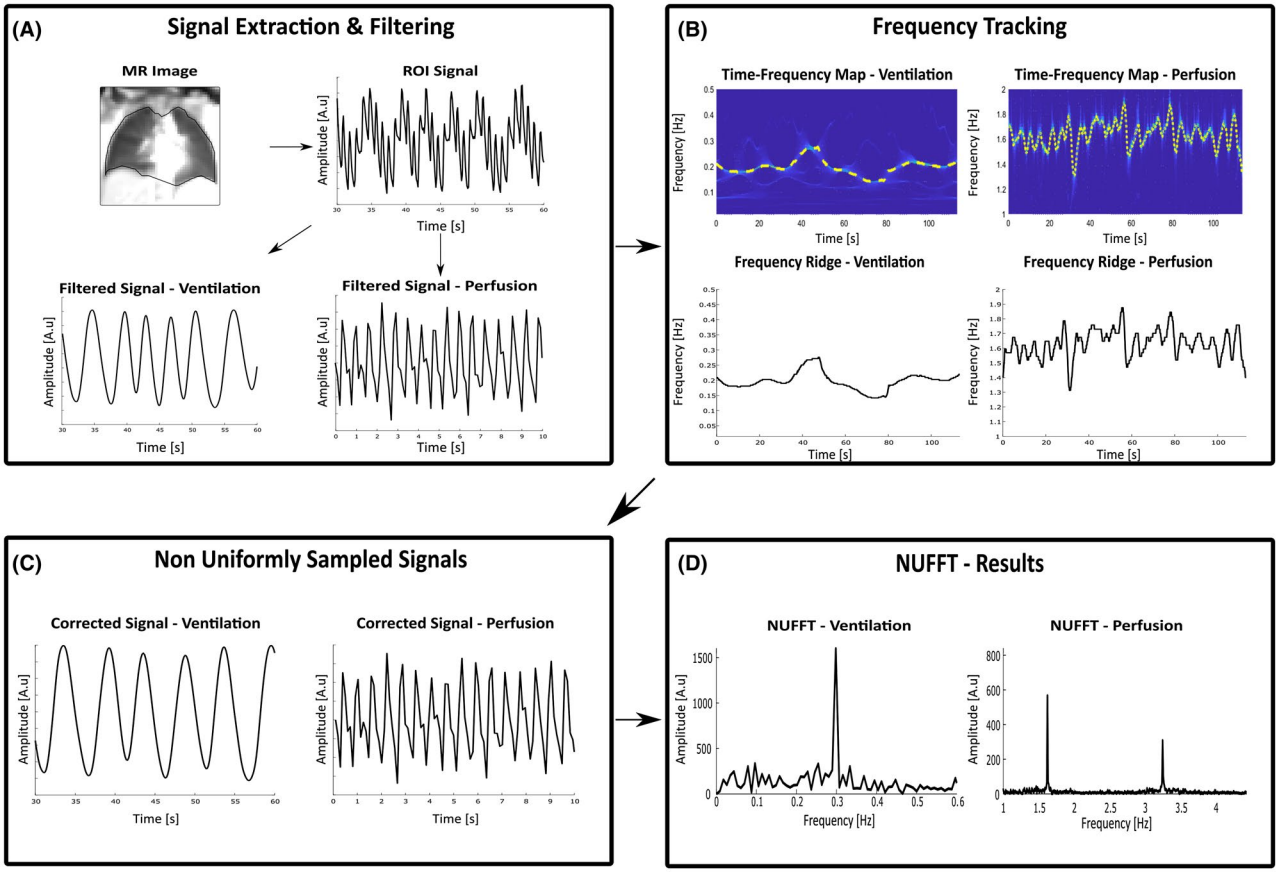

FIGURE 2 Workflow of NUFD MRI image processing. A, Extraction of ventilation and perfusion signal from large ROI by band-pass filtering. B, Resulting time-frequency map from SWT with tracked frequencies from ridge detection. C, Ventilation and perfusion signals displayed with recalculated sampling points (frequency variations are reduced in comparison to A. D, Resulting NUFFT spectra from the curves in C, showing that intensity has indeed been collected onto a single frequency bin for both ventilation and perfusion

which resulted in a 2D frequencies-over-time spectrum (time-frequency map in Figure 2B, top). For SWT, the analytical Morlet wavelet was selected as a mother wavelet over bump wavelet, due to its narrower variance in time dimension. To track the frequency of interest, a method called ridge detection can be used; e.g., the function "wsstridge" in Matlab.[16] Ridge detection (Figure 2B, bottom) follows the frequency of the maximum intensity signal component in the SWT spectrum by means of a penalized forward backward greedy algorithm. The penalty parameter limits large frequency jumps and was set to 0.3.

New "virtual" sampling times were then calculated with Equation 2, as described above (Figure 2C). Then, NUFFT was performed on the averaged lung ROI data, yielding 2 frequency spectra (1 for ventilation, 1 for perfusion), in which the relevant frequency bins for ventilation f_{vent} or perfusion f_{perf} could be determined (Figure 2D). The NUFFT was implemented[b] in Matlab with a Gaussian gridding based method,[17,18] which has shown to be yield better reconstruction performance for NUFFT estimations than methods combining other types of interpolation with standard FFT.[19]

Finally, ventilation- and perfusion-weighted *maps* were generated applying the NUFFT analysis (with the new sampling times determined above) for every lung voxel, similar as with the FD method. Amplitude maps were then calculated from the frequency spectra with the ventilation and perfusion frequencies f_{vent} and f_{perf} extracted from the averaged ROI time signal.

Using the complex phase of the spectral frequency bin of every voxel (after applying a 2D phase unwrapping algorithm,[20] another map termed "(signal) delay map" was generated showing the delay of the signal relative to a reference voxel. The actual time delay t_{delay} was calculated for each voxel as

$$t_{delay} = \frac{\phi_0 - \phi}{2\pi} T = \frac{\phi_0 - \phi}{2\pi f} \quad (5)$$

where ϕ is the phase angle, ϕ_0 is the phase of a reference voxel (with the highest phase value, i.e., lowest time delay in the analyzed ROI), and T is the cycle period, i.e., the inverse frequency $T = \frac{1}{f}$ of the ventilation or perfusion frequencies f_{vent} and f_{perf}.

For comparison, FD maps (with amplitude data and phase-based temporal delay data) were produced for all measurements.

3.3 | Image evaluation

A standard method for SNR calculation of Fourier transforms is to compare the amplitude of the signal frequency bin to the power of the noise frequency bins.[21] In the present study, SNR maps were calculated by dividing the signal of the ventilation and perfusion maps by the standard deviation of the noise bins of each lung voxel. The SNR maps were manually and separately segmented for both perfusion and ventilation evaluation. The perfusion ROI excluded the lower left lung where the heart moved into the section; the ventilation ROI excluded the large pulmonary vessels. To quantify and compare these SNR maps, the average SNR (mean value) within the ROI was then calculated. The percentage difference between SNR for the NUFD and FD method was then calculated. Statistical evaluation was lastly performed with 1-sample t-tests (2-tailed) on percentage change of SNR, for patient and volunteer measurements, respectively. Differences were considered to be statistically significant if *P*-values were less than 0.05.

4 | RESULTS

4.1 | SNR evaluation

Comparing NUFD to FD evaluation, a statistically significant increase of average ventilation and perfusion SNRs of healthy volunteers was found (including all measurements from the variable frequency test). Ventilation SNRs increased by $43.4\% \pm 25.3\%$ ($P < 0.001$) and perfusion SNRs by $93.0\% \pm 36.1\%$ ($P < 0.001$). The average increase of all eleven patients' ventilation and perfusion SNRs from NUFD compared to FD was also statistically significant with $24.4\% \pm 31.9\%$ ($P = 0.03$) and $75.6\% \pm 62.8\%$ ($P = 0.003$), respectively. All results are summarized in the Table 1.

Figure 3 displays an example of the resulting frequency spectra from the averaged ROI signal of a typical volunteer measurement, comparing the NUFD and FD approach. The spread-out frequency components of the FD approach have been collected and are clearly not overlapping in the NUFD results. In addition, both NUFD ventilation and perfusion have gained a clear increase of amplitude.

Figure 4 shows examples of SNR maps from the same measurement. Both ventilation and perfusion maps display substantially higher SNRs with the NUFD approach compared to the FD evaluation.

4.2 | Influence of frequency variability and volunteer data

Two of the resulting NUFD and FD maps from the repeated volunteer measurements with different ventilation frequency variability are presented in Figure 5. Improvements due to the NUFD approach were especially prominent in ventilation delay maps of measurement 2, in which the volunteer was asked to breathe very irregularly. Using the FD method

TABLE 1 SNR results for ventilation and perfusion measurements from FD and NUFD method displaying average and standard deviation SNR of volunteer and patient measurements

	SNR NUFD	SNR FD	SNR increase (absolute)	SNR increase (relative)	*P*-Value
Volunteer ventilation (n=11)	144.1 ± 32.6	102.7 ± 27.8	41.4 ± 17.7	43.4% ± 25.3%	2×10^{-5}
Volunteer perfusion (n=11)	52.3 ± 11.6	27.8 ± 6.8	24.5 ± 8.3	93.0% ± 36.1%	7×10^{-6}
Patients ventilation (n=11)	121.8 ± 64.5	95.1 ± 41.1	26.7 ± 36.3	24.4% ± 31.9%	3×10^{-2}
Patients perfusion (n=11)	18.5 ± 13.5	11.2 ± 7.5	7.3 ± 7.9	75.6% ± 62.8%	3×10^{-3}

Average and standard deviation increase in SNR (absolute and relative) between the 2 methods are also summarized with associated *P*-values.

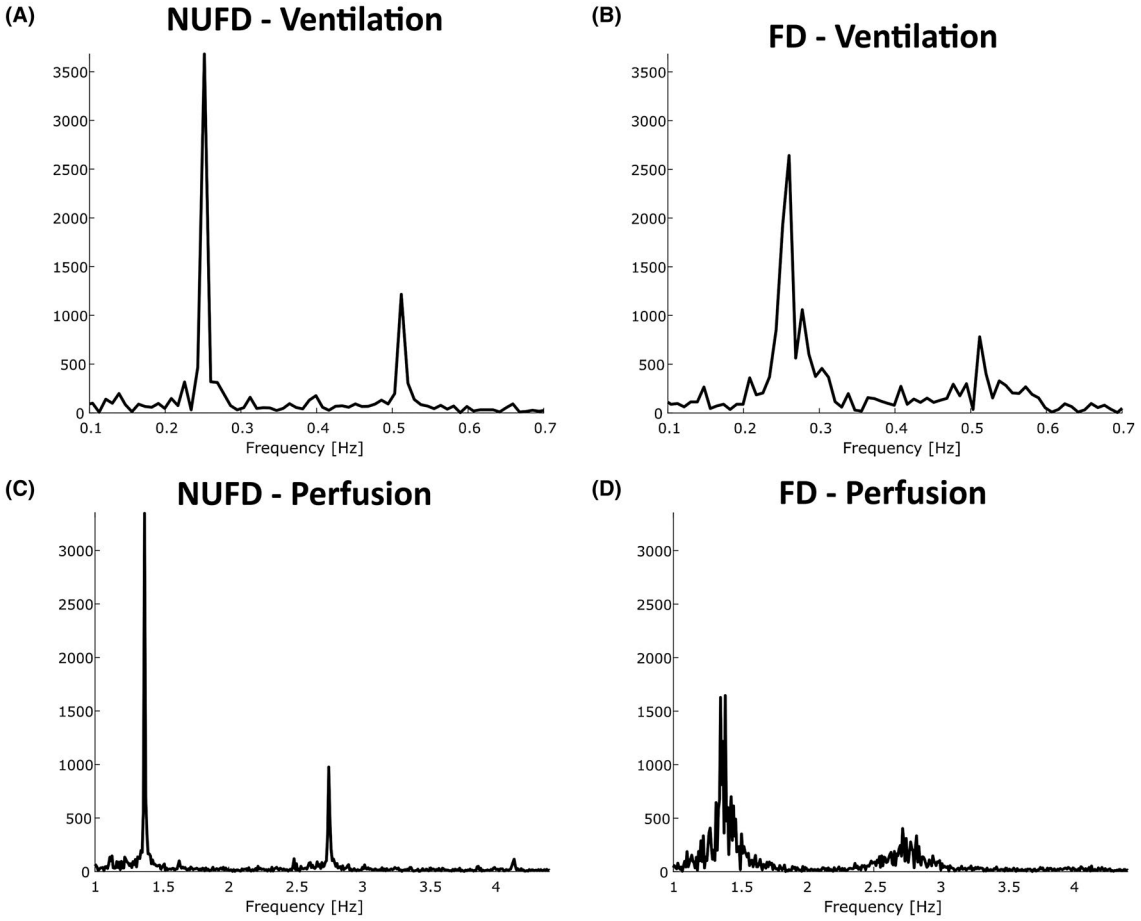

FIGURE 3 Frequency spectra from NUFD (A,C) and FD (B,D) MRI based on extracted and averaged ROI signal for ventilation (A,B) and perfusion (C,D) component

resulted in a different signal delay pattern in the ventilation case. Comparing the ventilation delay patterns between measurements 1 and 2, the NUFD map of measurement 2 was substantially more similar to measurement 1 than the FD maps. Generally, the perfusion delay maps illustrate consistently the propagation of the perfusion signal from the large central vessels to the pulmonary periphery.

In Table 2 below, a clearly improved average SNR is presented when comparing the NUFD and FD maps. However, it should be noted that the SNR increase was not linearly correlated with frequency variability. In fact, the highest ventilation frequency variability yielded the smallest increase in the estimation of measurement 2.

The NUFD delays of perfusion (i.e., $t_{\text{delay,max}} - t_{\text{delay,min}}$ within an individual map) ranged from 70 to 185 ms for the different volunteers (mean value over all volunteers was 126 ± 42.5 ms); for ventilation, the NUFD delays ranged from 180 to 370 ms (mean value was 280 ± 68.9 ms).

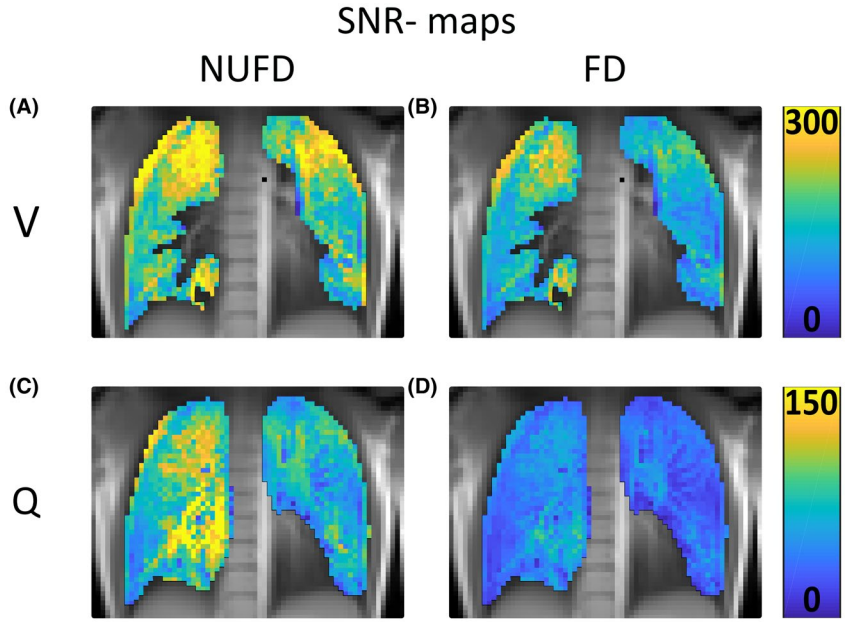

FIGURE 4 SNR maps generated from NUFD and regularly sampled FD spectra in a healthy volunteer. A,B, Ventilation (V) SNR maps displaying average SNRs of 195.3 and 144.2, respectively, corresponding to a +35.4% increase of SNR. C,D, Perfusion (Q) SNR maps displaying average SNRs of 80 and 39 corresponding to a +106% increase of SNR

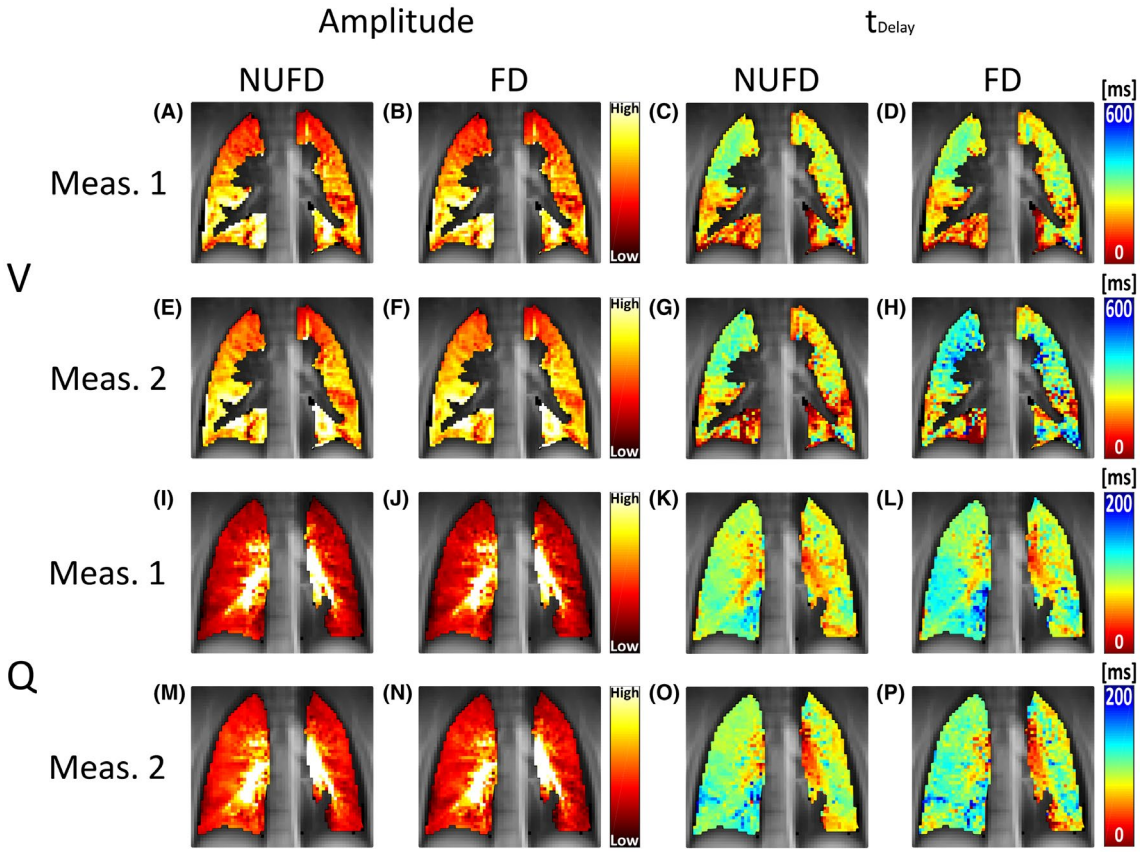

FIGURE 5 Influence of frequency variability. A-H, Ventilation-weighted (V) amplitude and signal delay maps from 2 measurements; the standard deviations of the ventilation frequencies were 0.01 Hz and 0.11 Hz, respectively. I-P, Perfusion-weighted (Q) amplitude and signal delay maps from 2 measurements; the standard deviations of cardiac frequencies were 0.04 Hz and 0.03 Hz, respectively

TABLE 2 Resulting average SNR from 6 measurements with varying frequency variability

	Ventilation						Perfusion					
	1	**2**	**3**	**4**	**5**	**6**	**1**	**2**	**3**	**4**	**5**	**6**
std (f) (Hz)	0.014	0.11	0.03	0.05	0.05	0.04	0.04	0.07	0.09	0.06	0.05	0.05
mean (f) (Hz)	0.12	0.20	0.15	0.20	0.14	0.14	0.95	1.04	0.96	1.04	0.96	0.99
mean(SNR_{FD})	96.6	99.7	82.4	72.4	82.4	91.9	35.1	21.0	27.1	21.7	32.4	27.1
mean(SNR_{NUFD})	144.8	103.3	111.8	127.9	111.2	130.2	66.0	47.6	43.8	52.9	43.5	48.9
increase (SNR)	48.2	3.5	29.4	55.5	28.8	38.3	30.9	26.6	16.8	31.2	11.1	21.8
increase (SNR) %	**50%**	**4%**	**36%**	**77%**	**35%**	**42%**	**88%**	**127%**	**62%**	**144%**	**34%**	**81%**

Table describes frequency variability std(*f*) (standard deviation of the tracked frequency) and mean frequency mean(*f*) for perfusion and ventilation signals with SNRs from FD and NUFD method as well as the absolute and relative SNR increase.

4.3 | Patient data

Two patients, 1 with suspicion of CTEPH and 1 with suspicion of PAH are presented in Figure 6. Both show large perfusion defects in the amplitude maps from both the FD and NUFD methods. However, when using the NUFD method, the SNR was increased in the perfusion maps for both measurements (from 11.5 to 19.6 in the CTEPH case, yielding 71% increase and from 7.2 to 10.7 in the PAH case, yielding 48% increase). This ensured that weaker blood pulsatility could be imaged in both cases, as can be seen, e.g., in Figure 6A,B,F,G. The PAH patient displayed a low but noticeable signal increase, homogenously spread in the left and right lung parenchyma with NUFD that could not be noticed with FD; the CTEPH patient showed stronger signal intensities in areas of the lower and upper right lung.

Increased SNR becomes also apparent when comparing the perfusion signal delay maps from FD and NUFD. For the PAH patient (Figure 6D,E), the NUFD delay map shows a smoother signal delay than the FD map, whose phase estimate is strongly distorted by noise.

5 | DISCUSSION

In this work, a new method for pulmonary Fourier-decomposition MRI based on the nonuniform Fourier transform was presented and applied for visualizing signal amplitudes and quantifying the signal delay in the lungs. It was demonstrated that, by adding a frequency-tracking step to the original FD method and switching perspective from variable signal frequency to variable sampling frequency, spectrally spread-out

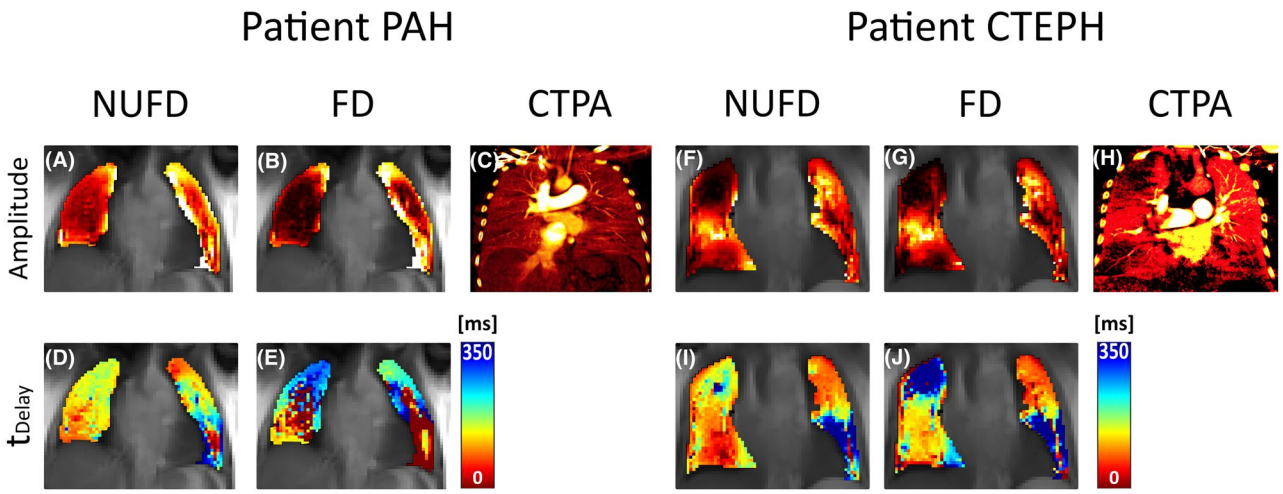

FIGURE 6 Perfusion-weighted NUFD and FD maps of patients with suspected PAH and CTEPH. A,B,F,G, FD and NUFD perfusion-weighted amplitude maps. D,E,I,J, Perfusion time delay maps. C,H, These 2 patients also had iodine-enhanced dual-energy CT pulmonary angiogram (CTPA) measurements (100/140Sn kV, 165/140 mAref, pitch = 1.2 for PAH patient and 90/150Sn kV, 60/46 mAref, pitch = 1.2 for CTEPH patient) performed as part of clinical routine within 3 months of their MR scans. The comparison shows that perfusion signal improvements from NUFD coincides better with displayed iodine concentration in both CTPA images. For the CTEPH patient, the CTPA image displays the decreasing, yet still existing signal intensity in the upper and lower part of the right lung where the lower part is stronger than the upper. This coincides better with the NUFD perfusion amplitude map than the one generated with FD

signal contribution could be collected onto a single frequency bin. This led to lessened bin spread caused by frequency variability as well as significant increase of SNR in both healthy test subjects and patient measurements, which can be expected to translate into more reliable quantitative results and less noisy parameter maps.

The patient measurements shown in Figure 6 clearly exemplify the difference NUFD can make for the evaluation of functional maps compared to FD. The effects are especially illustrated in the time delay maps comparing NUFD and FD, in which the PAH patient (Figure 6D,E) showed smoother progression and the CTEPH patient displayed further subtleties with better detectable signal progression (Figure 6I,J) in the upper right lung. In both cases, SNR was significantly improved. In the amplitude maps of the PAH patient (Figure 6A,B), the signal was substantially raised in voxels that had signal close to or lower than the noise floor (i.e., the local noise level of these voxels) with the FD method.

A key step of our new approach is frequency tracking of either the respiratory or the cardiac frequency during the 1 to 2 min of measurement. Current signal processing studies still discuss how best to describe signals with varying frequencies as amalgamation of multiple components and have specifically highlighted the influence of variable signal amplitudes.[22] Variable amplitudes are expected in biological signal variations (especially for ventilation-associated signals) and must be dealt with to avoid misleading added low frequency components. With this in mind, the SWT method was selected due to its implementation where a variable amplitude factor is added to the regular wavelet transform definition. In addition, SWT has also been shown to offer improved frequency localization in time compared with regular continuous wavelet transform.[23] The resulting time-frequency representation of the SWT approach also helps to spread out potential artifacts and noise over the 2D frequency-time spectrum resulting in more stable estimates than those performed only in the (1D) time domain.

Because the NUFD method requires no changes in image acquisition parameters, it can easily be implemented as a complement to ongoing and future studies. The tracking of the (free-breathing) respiratory frequency offers fewer limitations for patient selection compared to regular FD MRI, as even patients strongly suffering from their conditions, which have troubles to breathe regularly, can be examined.

Due to the possibility of determining the signal delay with high temporal resolution from phase estimates, time delay maps can be calculated to estimate how the perfusion or respiratory signal propagates through microstructures in the lungs. However, further studies are required to validate the resulting delay maps quantitatively. The measured range of ventilation delays throughout the lungs of healthy subjects was between approximately 180 and 370 ms. This agrees well with results from a dynamic spiral MRI study,[24] in which similar values were shown for the gas delay during inhalation.

Similar to PREFUL[10] and SENCEFUL,[9] the proposed NUFD method generates functional maps where all of the signal contribution collected during the measurement can be used. Because the same amount of signal is used for the evaluation, one would expect similar SNR increases with the NUFD approach as with the 2 other methods compared to FD. NUFD MRI, however, distinguishes itself in that it does not require exact phase estimates for performing image or k-space line resorting, thus simplifying the final implementation.

There are some limitations of this study. First, the proposed NUFD approach requires an additional (in comparison to FD MRI) frequency-tracking step. There exist several approaches for frequency tracking and here we used the SWT in combination with ridge detection. Further studies should compare this technique with other approaches (such as, e.g., frequency tracking by simple peak finding) to determine the most robust and reliable technique. Second, even without frequency variability, NUFD MRI can suffer from the same amplitude stability issues as was described for FD MRI,[25] for which solutions such as windowing[21] or matrix pencil decomposition,[25] are readily available. Thus, NUFD estimates of both amplitude and phase can be expected to be further improved upon with an optimal choice of a filtering window function. However, because the focus of this study was to compare the results between NUFD and FD MRI (where windowing is not an efficient option due to the predominant influence of frequency variability in vivo), this was left out for future investigations. Furthermore, this is a proof of principle study and future studies with larger sample size are required to establish clinical relevance of the found SNR improvements. Finally, it should be noted that because imaging is performed in 2D, artifacts can occur as with the regular FD method due to movement of structures in an out of the slice which would likely occur at ventilation rate.

6 | CONCLUSIONS

This study presents a modification of functional Fourier-decomposition lung imaging with frequency-adapted Fourier transform to compensate for variability in perfusion and ventilation frequency. We demonstrated that using nonuniform Fourier transform in combination with frequency tracking can significantly increase SNR and reduce frequency overlaps by collecting the signal intensity onto single frequency bins.

ACKNOWLEDGMENT

We thank Dr. Oliver Bieri (Universitätsspital Basel, Switzerland) for his work on optimizing the uf-bSSFP sequence.

CONFLICT OF INTEREST

Thomas Gaass is currently employed by Siemens Healthcare Pty Ltd, Bowen Hills, Australia. Bernd Kühn is currently employed by Siemens Healthcare GmbH, Erlangen, Germany.

ENDNOTES

[a] Generally, 3 types of NUFFT algorithms are differentiated: (1) Type-1 NUFFTs perform a spectral analysis of data sampled at nonequidistant time points resulting in an equidistantly defined frequency spectrum; (2) type-2 NUFFTs perform a spectral analysis of equidistantly sampled data resulting in a nonequidistantly defined frequency spectrum; (3) type-3 NUFFTs combine type-1 and type-2 NUFFT, namely transforming a nonequidistantly sampled signal to a nonequidistantly defined frequency spectrum.

[b] Code initially written by M. Ferrara at AFRL Sensors Directorate Innovative Algorithms Branch.

REFERENCES

1. Bauman G, Puderbach M, Deimling M, et al. Non-contrast-enhanced perfusion and ventilation assessment of the human lung by means of Fourier decomposition in proton MRI. *Magn Reson Med*. 2009;62:656–664.
2. Kjørstad Å, Corteville DMR, Fischer A, et al. Quantitative lung perfusion evaluation using Fourier decomposition perfusion MRI. *Magn Reson Med*. 2014;72:558–562.
3. Zapke M, Topf H-G, Zenker M, et al. Magnetic resonance lung function–a breakthrough for lung imaging and functional assessment? A phantom study and clinical trial. *Respir Res*. 2006;7:106.
4. Martirosian P, Boss A, Fenchel M, et al. Quantitative lung perfusion mapping at 0.2 T using FAIR True-FISP MRI. *Magn Reson Med*. 2006;55:1065–1074.
5. Bauman G, Scholz A, Rivoire J, et al. Lung ventilation- and perfusion-weighted Fourier decomposition magnetic resonance imaging: in vivo validation with hyperpolarized 3He and dynamic contrast-enhanced MRI. *Magn Reson Med*. 2013;69:229–237.
6. Bauman G, Lützen U, Ullrich M, et al. Pulmonary functional imaging: qualitative comparison of Fourier decomposition MR imaging with SPECT/CT in porcine lung. *Radiology*. 2011;260:551–559.
7. Bauman G, Eichinger M, Uecker M. High temporal resolution radial bSSFP sequence with nonlinear inverse reconstruction for the measurement of the pulmonary blood inflow time using Fourier decomposition MRI. In: Proceedings of the 20th Annual Meeting of ISMRM, Melbourne, Australia, 2012. Abstract 1340.
8. Veldhoen S, Weng AM, Wirth C, et al. Pulmonary phase imaging using self-gated Fourier decomposition MRI in patients with cystic fibrosis. In: Proceedings of the 24th Annual Meeting of ISMRM, Singapore, 2016. Abstract 114.
9. Fischer A, Weick S, Ritter CO, et al. SElf-gated Non-Contrast-Enhanced FUnctional Lung imaging (SENCEFUL) using a quasi-random fast low-angle shot (FLASH) sequence and proton MRI. *NMR Biomed*. 2014;27:907–917.
10. Voskrebenzev A, Gutberlet M, Klimeš F, et al. Feasibility of quantitative regional ventilation and perfusion mapping with phase-resolved functional lung (PREFUL) MRI in healthy volunteers and COPD, CTEPH, and CF patients. *Magn Reson Med*. 2018;79:2306–2314.
11. Bieri O. Ultra-fast steady state free precession and its application to in vivo (1)H morphological and functional lung imaging at 1.5 tesla. *Magn Reson Med*. 2013;70:657–663.
12. Hirsch JA, Bishop B. Respiratory sinus arrhythmia in humans: how breathing pattern modulates heart rate. *Am J Physiol*. 1981;241:H620–H629.
13. Chefd'hotel C, Hermosillo G, Faugeras O. Flows of diffeomorphisms for multimodal image registration. In: Proceedings IEEE International Symposium on Biomedical Imaging, Washington, DC, 2002:753–756.
14. Chefd'Hotel C, Hermosillo G, Faugeras O. A variational approach to multi-modal image matching. In: Proceedings IEEE Workshop on Variational and Level Set Methods in Computer Vision, Vancouver, BC, Canada, 2001:21–28.
15. Daubechies I, Lu J, Wu H-T. Synchrosqueezed wavelet transforms: an empirical mode decomposition-like tool. *Appl Comput Harmon Anal*. 2011;30:243–261.
16. Carmona RA, Hwang WL, Torresani B. Characterization of signals by the ridges of their wavelet transforms. *IEEE Trans Signal Process*. 1997;45:2586–2590.
17. Greengard L, Lee J. Accelerating the nonuniform fast Fourier transform. *SIAM Rev*. 2004;46:443–454.
18. Liu QH, Nguyen N. An accurate algorithm for nonuniform fast Fourier transforms (NUFFT's). *IEEE Microw Guid Wave Lett*. 1998;8:18–20.
19. Zhang K, Kang JU. Graphics processing unit accelerated nonuniform fast Fourier transform for ultrahigh-speed, real-time Fourier-domain OCT. *Opt Express*. 2010;18:23472.
20. Goldstein RM, Zebker HA, Werner CL. Satellite radar interferometry: two-dimensional phase unwrapping. *Radio Sci*. 1988;23:713–720.
21. Harris FJ. On the use of windows for harmonic analysis with the discrete Fourier transform. *Proc IEEE*. 1978;66:51–83.
22. Huang NE, Shen Z, Long SR, et al. The empirical mode decomposition and the Hilbert spectrum for nonlinear and non-stationary time series analysis. *Proc R Soc Lond Math Phys Eng Sci*. 1998;454:903–995.
23. Thakur G, Brevdo E, Fučkar NS, Wu H-T. The Synchrosqueezing algorithm for time-varying spectral analysis: robustness properties and new paleoclimate applications. *Signal Process*. 2013;93:1079–1094.
24. Salerno M, Altes TA, Brookeman JR, de Lange EE, Mugler JP. Dynamic spiral MRI of pulmonary gas flow using hyperpolarized (3)He: preliminary studies in healthy and diseased lungs. *Magn Reson Med*. 2001;46:667–677.
25. Bauman G, Bieri O. Matrix pencil decomposition of time-resolved proton MRI for robust and improved assessment of pulmonary ventilation and perfusion. *Magn Reson Med*. 2017;77:336–342.

How to cite this article: Bondesson D, Schneider MJ, Gaass T, et al. Nonuniform Fourier-decomposition MRI for ventilation- and perfusion-weighted imaging of the lung. *Magn Reson Med*. 2019;82:1312–1321. https://doi.org/10.1002/mrm.27803